

Effect of Mg/Si mass ratio on microstructure and mechanical properties of Al-Mg-Si cast aluminum alloy

Jia-yan Chen^{1,2}, Ce Zheng², Cheng Zhu², Ying-ju Li², *Tian-jiao Luo², **Cui-rong Liu^{1,3}, Shao-qiang Xu⁴, and Yuan-sheng Yang²

1. School of Material Science and Engineering, Taiyuan University of Science and Technology, Taiyuan 030024, China

2. Shi-changxu Innovation Center for Advanced Material, Institute of Metal Research, Chinese Academy of Sciences, Shenyang 110016, China

3. Preparatory Department, Modern College of Humanities and Sciences, Shanxi Normal University, Linfen 041000, Shanxi, China

4. WQ & UCAS (Binzhou) Industrialization Research Institute Co., Ltd., Binzhou 256699, Shandong, China

Copyright © 2025 Foundry Journal Agency

Abstract: The effect of Mg/Si mass ratio on the microstructure and mechanical properties of Al-Mg-Si cast aluminum alloys under sub-rapid solidification conditions was investigated. This study utilized four different Mg/Si ratios: 2.83, 1.91, 1.73, and 1.53. To analyze the evolution of the microstructure, particularly the second phase, various techniques were employed: optical microscopy (OM), scanning electron microscopy (SEM), energy dispersive spectrometry (EDS), and electron backscatter diffraction (EBSD). Additionally, thermodynamic calculations were performed using the Thermal-calc software to further understand the microstructural changes. Results show that as the Mg/Si ratio decreases from 2.83 to 1.53, α -Al grains become more uniformly distributed. Meanwhile, the morphology of the Mg_2Si phases changes from skeletal to short stick shapes with a decreasing aspect ratio. An as-cast Al-Mg-Si alloy with a Mg/Si ratio of 1.53 exhibits high strength, achieving an ultimate tensile strength (UTS) of 320.6 MPa and a yield strength (YS) of 249.9 MPa. The cast alloy with a Mg/Si ratio of 2.83 exhibits the highest elongation, reaching 5.31%. This superior elongation is attributed to the uniform distribution of Mg_2Si phases, which possess a long skeletal shape. Conversely, the alloy with a Mg/Si ratio of 1.53 demonstrates the lowest elongation, primarily due to the central concentration of Mg_2Si phases, which are characterized by their short stick shapes.

Keywords: Al-Mg-Si casting alloys; Mg/Si mass ratio; dendrite arm spacing; Mg_2Si phase; mechanical properties

CLC numbers: TG146.21

Document code: A

Article ID: 1672-6421(2025)02-163-10

1 Introduction

The advancement of large-scale integrated die-casting technologies has led to the increased use of aluminium alloy structural components in automotive bodies [1-2]. However, the large-sized and thin-walled components are easy to deform during heat treatment. This necessitates those aluminium alloys possess excellent mechanical

properties in the as-cast state. The Al-Mg-Si alloy, known as Magsimal-59, is notable for its superior casting capabilities and mechanical properties. Nevertheless, as usage demands continue to escalate, the strength of Al-Mg-Si alloy may no longer satisfy these higher requirements.

Microalloying with elements such as Cu or Zr and adjusting the content of the main elements (Mg/Si ratio) [3-7] are the main methods to improve the mechanical properties of cast alloys. However, the addition of Cu increases the hot cracking susceptibility of the alloy. Although the addition of Zr can refine the grains, it generates the coarse incipient phase. Adjusting the Mg/Si ratio is a cost-effective method to improve the mechanical properties of alloys. The stoichiometric ratio for the formation of Mg_2Si phase is 2:1 for Mg and Si elements, respectively, which means the critical

*Tian-jiao Luo

Male, Ph. D., Associate Professor. His research interests mainly focus on the preparation and properties of new magnesium and magnesium alloy/aluminum and aluminum alloy materials.

E-mail: tjluo@imr.ac.cn

**Cui-rong Liu

E-mail: 2006042@tyust.edu.cn

Received: 2023-09-04; Revised: 2024-06-08; Accepted: 2024-07-10

mass ratio of Mg/Si is 1.73:1. If the actual mass ratio of Mg to Si in the alloy is less than 1.73:1, it indicates that there is an excess of Si in the alloy. The excess Si can lower the Mg/Si mass ratio of G.P. zones and β'' phases, promote the precipitation of β'' phases and enhance the age-strengthening, leading to an excellent strength^[8], high corrosion resistance^[9], and high thermal conductivity^[10]. If the mass ratio of Mg/Si is larger than 1.73, it indicates that there is an excess of Mg in the alloy. The excess Mg elements are dissolved into the α -Al matrix at a high cooling rate of the die-casting process, resulting in substantial enhancement of strength for α -Al matrix^[11]. Until now, there has been a lack of comprehensive and quantitative research exploring how the Mg/Si ratio influences the mechanical properties of die-cast Al-Mg-Si alloys, especially under the sub-rapid solidification conditions typical of the die-casting process. Sub-rapid solidification is characterized by cooling rates that can reach 10^0 - 10^3 K·s⁻¹^[12-14]. This rapid cooling can significantly affect the microstructure and hence the mechanical properties of the alloy.

In this work, the effects of Mg/Si mass ratio on the mechanical properties of Al-Mg-Si negative pressure suction casting alloys were systematically investigated under sub-rapid solidification conditions. The study also examined the morphology and distribution of Mg₂Si phases within the alloys. Furthermore, the investigation included a calculation of the respective contributions made by Mg and Si elements to the strengthening mechanisms of the alloys.

2 Experimental procedure

The four Al-Mg-Si-based alloys with different Mg/Si ratios (2.83, 1.91, 1.73, 1.53, wt.%) were prepared using 99.95wt.% pure Al,

99.95wt.% pure Mg, pure Fe, Al-20wt.% Si, Al-10wt.% Mn, Al-5wt.% Ti, and Al-4wt.% Zr. Before melting, all the raw materials were polished to avoid the oxide skins on the surfaces, and then stored in the preheated furnace at 200 °C for 12 h to remove the moisture. During melting, pure Al blocks were heated to 740 °C-750 °C in an intermediate frequency induction furnace. Then, Al-20wt.% Si, Al-10wt.% Mn, Al-5wt.% Ti, and Al-4wt.% Zr master alloys were added at 780 °C, 760 °C, 740 °C, and 720 °C, respectively, and holding for 10 min. When the temperature of the melts decreased to 710 °C-720 °C, pure Mg blocks were pressed under the melt surface by using a graphite hood to prevent being floated and burned. After the melting was completed, the modifier of Al-10wt.% Sr and refiner of Al-5Ti-1B were added to the melt and held for 20 min. After degassing with C₂Cl₆ powder for 5 min, the Al-Mg-Si melt, at 710 °C, was poured into a copper mold preheated to 200 °C by negative pressure suction casting, as shown in Fig. 1. The negative pressure was 0.9 MPa. The actual chemical composition of the as-cast Al-Mg-Si alloys was analyzed using a photoelectric direct reading spectrometer (QSG-750-II), as listed in Table 1.

The OM, SEM, and EBSD were carried out to characterize the microstructure of as-cast Al-Mg-Si samples. All the observation regions were selected at the cross-section of as-cast samples. For OM and SEM samples, the as-cast alloys were mechanical ground and polished on the LaboPol-6 metallographic machine, and then etched in a Keller's reagent (95 mL H₂O, 2.5 mL HNO₃, 1.5 mL HCl, 1.0 mL HF) for 30 s-60 s. The metallographic analysis was carried out by using a ZEISS Axio Observer.Z1m microscopic analysis system. The EBSD specimens were further ion cleaned by Leica 101 operated with a scanning angle of 6°-12° for 60 min, under the scanning step size of 2.0 μ m. All the EBSD data were analyzed using the

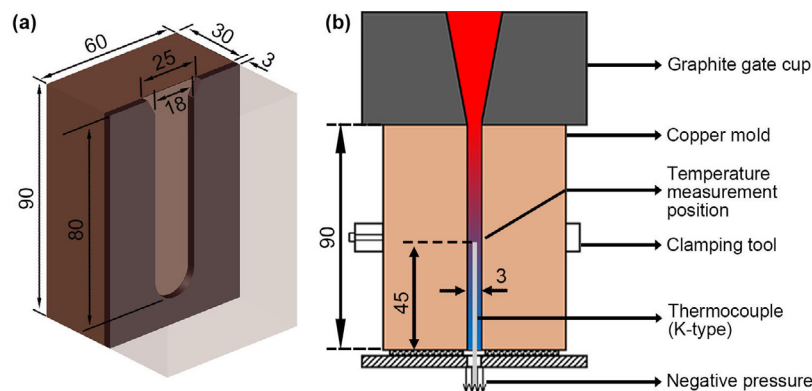


Fig. 1: Schematic diagram of copper U-shaped through slot mold (mm) (a) and negative pressure suction casting mold assembly (b)

Table 1: Chemical compositions (wt.%) of as-cast Al-Mg-Si alloys with various Mg/Si ratios

Mg/Si	Mg	Si	Ti	Mn	Fe	Zr	Al
2.83	6.31	2.23	0.13	0.62	0.22	0.060	Bal.
1.91	4.88	2.56	0.11	0.65	0.21	0.051	Bal.
1.73	4.45	2.58	0.14	0.67	0.17	0.062	Bal.
1.53	4.20	2.74	0.13	0.65	0.18	0.059	Bal.

HKL Channel 5 software.

The tensile experiment was carried out on the AG-Xplus100KN universal tensile machine at room temperature with a tensile speed of 1.44 mm·min⁻¹. The dog-bone-shaped tensile samples with a parallel length of 24 mm and a thickness of 3 mm were cut from as-cast specimens (Fig. 2). For each alloy, three

experiments were performed and the average values of yield strength (YS), ultimate tensile strength (UTS), and elongation to failure were recorded. To investigate the fracture behavior and mechanism of the alloys, analysis was conducted using a JSM-6301F scanning electron microscope (SEM) equipped with an Oxford EDS-500 energy spectrum analyzer.

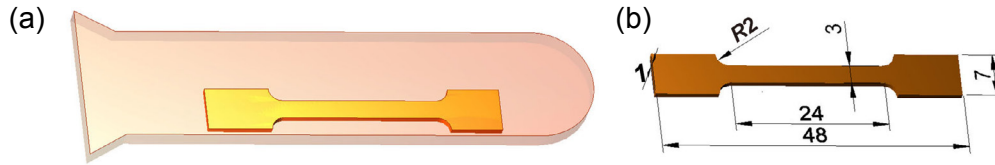


Fig. 2: Preparation of room temperature tensile samples: (a) sampling location; (b) sample sizes (Unit: mm)

3 Results and discussion

3.1 Measurement and calculation of cooling rate

The cooling rate of the suction casting experiment was measured by inserting a thermocouple, as shown in Fig. 1(b). The rapid cooling of the sample resulted in a temperature curve that did not capture the peak temperature. To address this issue and obtain the missing maximum temperature data, ProCAST software was employed to simulate the temperature field during the solidification process of the Al-Mg-Si alloy samples. The temperature data obtained from the simulation at different solidification moments were compared with the experimental results, as shown in Fig. 3. The correlation coefficient r between experimental temperatures and the simulation results at the corresponding moments was calculated by using Eq. (1):

$$r = \frac{\sum(x - \bar{x})(y - \bar{y})}{\sqrt{\sum(x - \bar{x})^2 \sum(y - \bar{y})^2}} \quad (1)$$

where r is the Pearson correlation coefficient, x and y are the temperature results obtained by the experimental and simulation methods, respectively, at the corresponding points in time, \bar{x} and \bar{y} are the mean values of the temperatures obtained through the experimental and simulation methods,

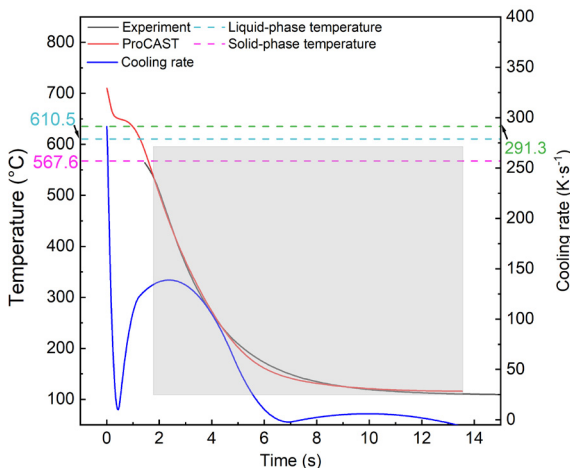


Fig. 3: Comparison of the experimental cooling curve and simulated results

respectively. If r is close to 1, it indicates a strong positive correlation between the two sets of variables; if r is close to -1, it indicates a strong negative correlation between the two sets of variables; and if r is close to 0, it indicates no linear relationship between the two sets of variables. The results show a strong correlation between the two curves with a correlation coefficient of 0.99, which suggests that simulation results can replace the undetected part of the experimental curve with a certain credibility.

The average cooling rate of the alloy during solidification (from maximum temperature to solid phase temperature of 567.6 °C) can be obtained by Eq. (2) as 137.5 K·s⁻¹.

$$k_{\text{aver.}} = \frac{T_1 - T_s}{t_s} \quad (2)$$

where $k_{\text{aver.}}$ is the average cooling rate during solidification, T_1 is the liquid phase temperature of Al-Mg-Si alloy (610.5 °C), T_s is the solid phase temperature of the alloy (567.6 °C), and t_s is the solidification time.

The maximum cooling rate calculated by Eq. (3) is 291.3 K·s⁻¹, which falls within the cooling rate range of the sub-rapid solidification process (1 K·s⁻¹-10³ K·s⁻¹).

$$k_{\text{max.}} = \max_{t_0 < t < t_1} \left| \frac{dT}{dt} \right| \quad (3)$$

where T is temperature, t is time, $k_{\text{max.}}$ is the tangent slope between the maximum temperature and solid phase temperatures in the cooling section of the cooling curve, t_0 is the time corresponding to the maximum temperature point, and t_1 is the time corresponding to the solid phase temperature point.

3.2 Effect of Mg/Si mass ratio on microstructure of as-cast alloy

The secondary dendrite arm spacing (SDAS) was measured by Image-Pro Plus according to the method shown in Fig. 4. The average SADS is calculated according to Eq. (4):

$$\lambda = \left(\frac{l_1}{m_1 - 2} + \frac{l_2}{m_2 - 2} + \dots + \frac{l_n}{m_n - 2} \right) / n \quad (4)$$

where λ is the average secondary dendrite arm spacing (μm); l_n is the distance between the first side-branch to the last

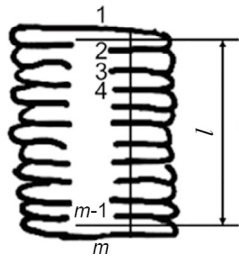


Fig. 4: Schematic diagram of secondary dendrite spacing measurement

one of a measured dendrite group (μm); m_n is the number of intersections between dendrites and the line connecting both ends of a measured dendrite group; (m_n-2) is the number of dendrites; and n is the number of measured dendrite groups.

The grain size and SDAS distribution of the α -Al grains were obtained from the EBSD and OM results, as shown in Fig. 5. The grain size shows minimal variation at Mg/Si ratios of 2.83 and 1.91, measuring 42.45 μm and 40.65 μm , respectively. However, when the Mg/Si ratio decreases to 1.73, the grain size reaches a maximum of 52.54 μm . A further reduction to 1.53 results in a

decrease to 43.95 μm . When the Mg/Si exceeds the critical value of 1.73 for the formation of Mg_2Si phases, the average grain size is decreased with further decrease of Mg/Si ratio, and at the same time, the microstructure of as-cast alloys becomes more homogeneous. In addition, the average SDAS value of the α -Al matrix fluctuates within a range of only 7 μm to 8 μm , indicating that there is no significant correlation with the Mg/Si ratio.

3.3 Effect of Mg/Si mass ratio on second phase of as-cast alloy

The influence of Mg/Si mass ratio on solidification path of Al-Mg-Si as-cast alloys was investigated by using Thermal-calc software, and the phase constitutions were obtained, as shown in Fig. 6. When the Mg/Si mass ratio is 2.83, the Mg element is relatively excess resulting in the formation of Al_3Mg_2 and Mg_2Si phases. When Mg/Si is 1.53, the Si element is relatively excessive, leading to the formation of Mg_2Si phases and eutectic Si. With the decrease of Mg/Si (in other words the increase of Si), some Si-containing phases formed, such as π - $\text{Al}_8\text{FeMg}_3\text{Si}_6$ and $\text{Al}(\text{Fe, Mn})\text{Si}$.

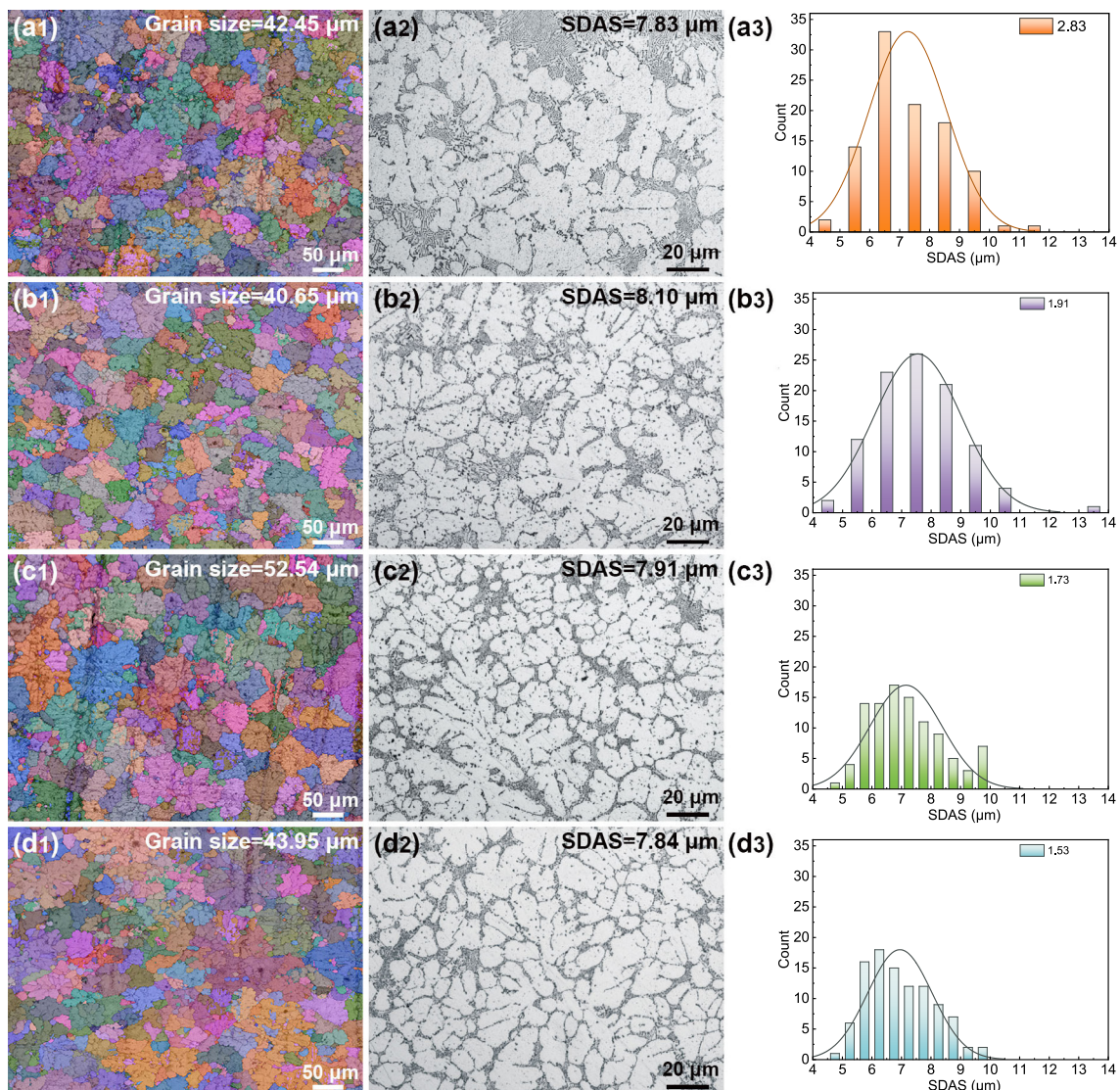


Fig. 5: EBSD results (a1-d1), OM figures (a2-d2), and SDAS distribution (a3-d3) of alloys with Mg/Si ratio of 2.83 (a1-a3), 1.91 (b1-b3), 1.73 (c1-c3), and 1.53 (d1-d3)

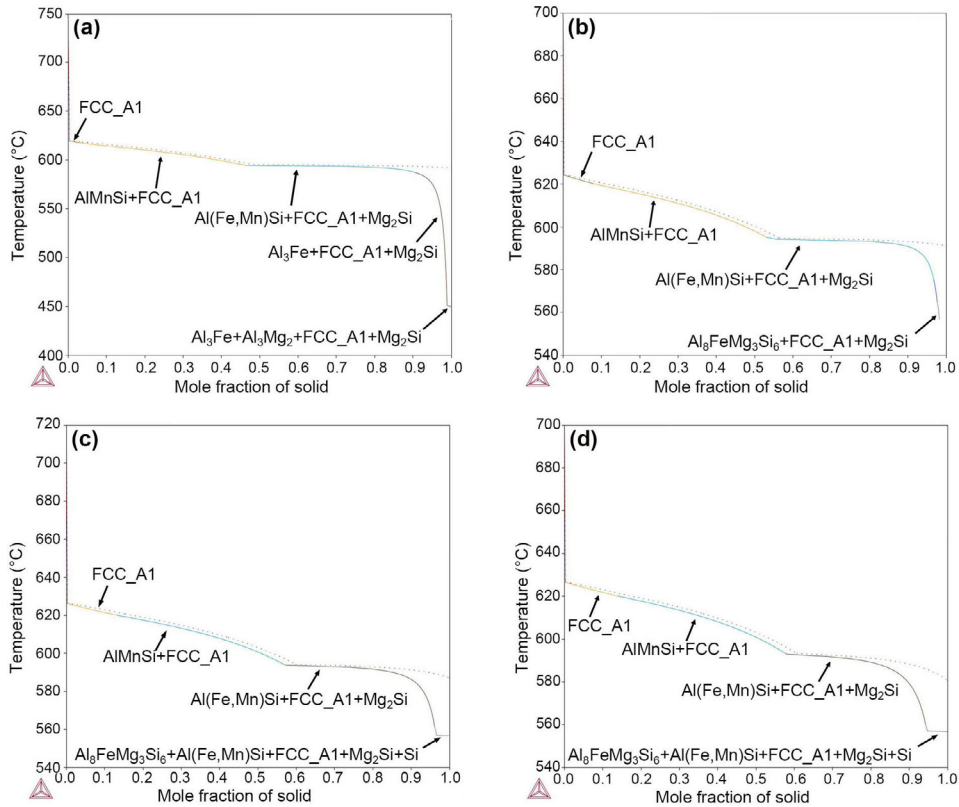


Fig. 6: Temperature-phase constitution of the alloys with different Mg/Si mass ratios: (a) 2.83; (b) 1.91; (c) 1.73; (d) 1.53

Figure 7 shows the SEM images and aspect ratios of the Mg_2Si phases in the four Al-Mg-Si alloys with different Mg/Si mass ratios. To investigate the effect of the Mg/Si on the morphology of the Mg_2Si phases, the aspect ratios of the Mg_2Si phases were measured using Image-Pro Plus software under the same magnification. For each alloy, 10 figures were measured and at least 200 data were obtained. Then, the measurement results were counted, as shown in the right column of Fig. 7.

From the SEM results in Fig. 7, it is observed that the morphology of the Mg_2Si phase gradually changes from long

skeletal shape to short stick or worm shape as the Mg/Si ratio decreases from 2.83 to 1.73. When the Mg/Si ratio is 1.53, the Mg_2Si phase exhibits a short skeletal shape. This is consistent with the results of Huang^[15] and Yan^[16] et al. When the Mg/Si ratio drops from 2.83 to 1.91, the proportion of Mg_2Si phases with an aspect ratio below 10 increases from 55.09% to 70.55%. However, as the Mg/Si ratio decreases from 1.91 to 1.53, the proportion decreases from 70.55% to 64.91%. Therefore, the Al-Mg-Si alloy contains more refined Mg_2Si phases when the Mg/Si ratio is within the range of 1.73 to 1.91.

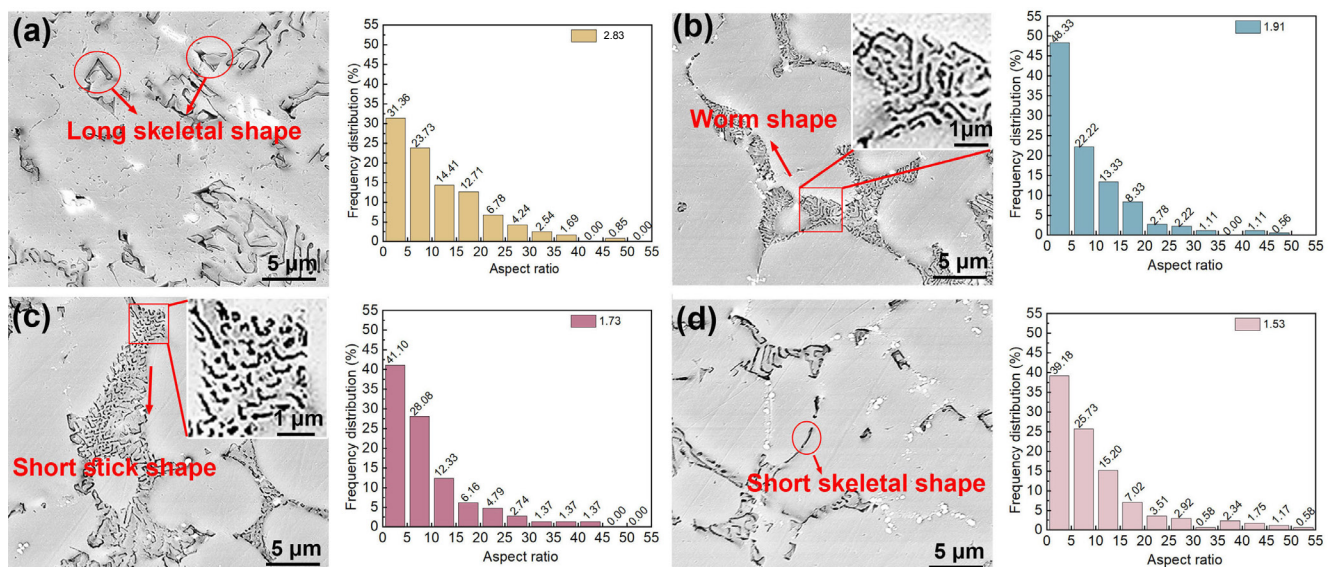


Fig. 7: Mg_2Si morphology and aspect ratio distribution of the four Al-Mg-Si alloys with different mass ratios of Mg/Si: (a) 2.83; (b) 1.91; (c) 1.73; (d) 1.53

Figure 8 illustrates the volume fraction of the Mg₂Si phase in four Al-Mg-Si alloys. Among these alloys, it can be seen that the proportion of the Mg₂Si phase is maximized when the Mg/Si ratio is 1.73.

Some white block phases are observed in the SEM backscattering figures, as shown in Figs. 9(a)-(d). These intermetallic phases are indexed in the SEM-EDS, as shown in Figs. 9(a, e), which are proved to be α-Al(Fe, Mn)Si phases. This means that the Mn element transforms the β-Fe phase into the α-Fe phase, reducing the detrimental effect of the needle-

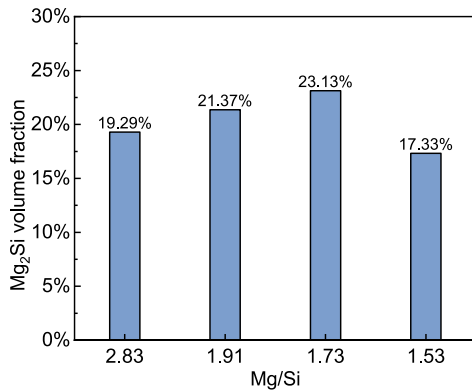


Fig. 8: Volume fraction of Mg₂Si phase

like β-Fe phase on the matrix [17]. In addition, as the mass ratio of Mg/Si decreases, the distribution pattern of α-Al(Fe, Mn)Si phases gradually changes from a dispersed distribution throughout the matrix to an alignment along the grain boundaries.

The EDS results in Figs. 9(d, f) show that the white particles are also the α-Al(Fe,Mn)Si. According to the research results of Sang et al. [18], the phases at the grain boundary in the alloy are related to the content of Si. As the Mg/Si ratio diminishes from 2.83 to 1.53, the concentration of Si rises, making the precipitation of α-Al(Fe,Mn)Si phase particles at grain boundaries more probable. This is due to the high interfacial energy present at the grain boundaries and the lower bonding energy, which makes the Si-rich phase more prone to nucleation along these areas [9].

3.4 Effect of Mg/Si mass ratio on mechanical properties of as-cast alloys

Figure 10 shows the mechanical properties of the four Al-Mg-Si alloys with different mass ratios of Mg/Si. It can be seen that when the Mg/Si is 1.53 (excess Si), the mechanical properties of the alloys are better: the UTS is 320.6 MPa, YS is 249.9 MPa, and the elongation reaches 2.31%. As Mg/Si gradually increases to 2.83, the UTS decreases to 297.8 MPa, with a reduction of

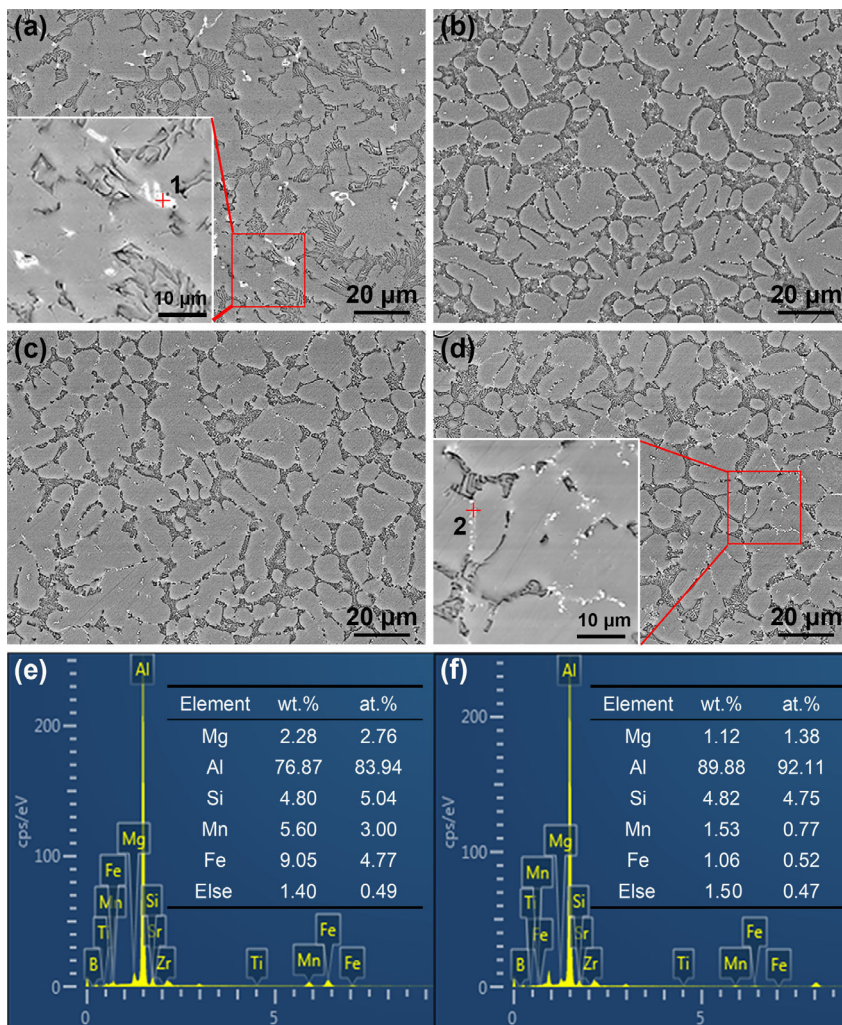


Fig. 9: SEM backscattered morphology of four alloys with different Mg/Si mass ratios: (a) 2.83; (b) 1.91; (c) 1.73; (d) 1.53; (e) energy spectrum analysis of Point 1; (f) energy spectrum analysis of Point 2

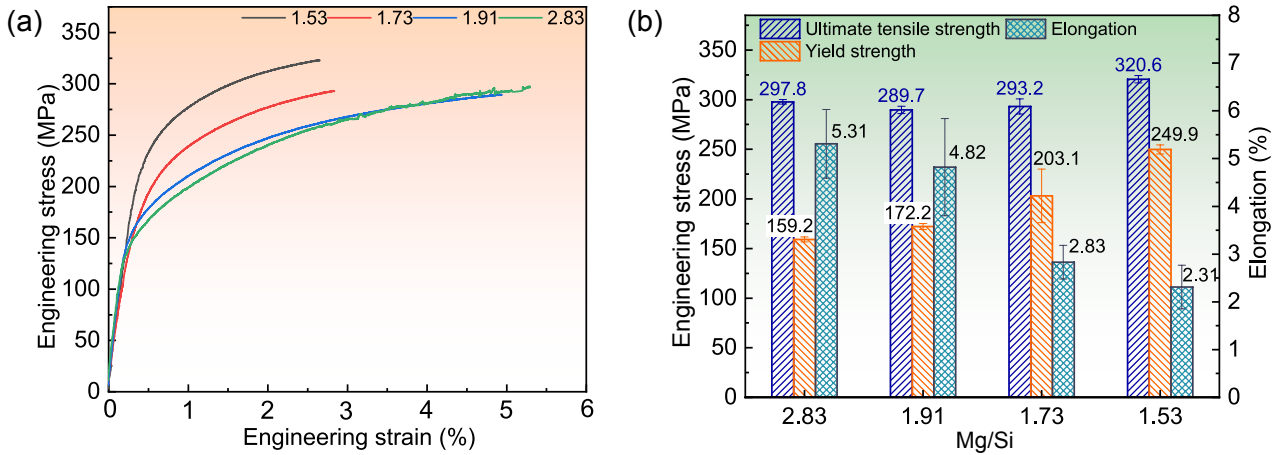


Fig. 10: Stress-strain curves (a) and mechanical properties (b) of alloys with different Mg/Si mass ratios at room temperature

7.11%, and the YS decreases to 159.2 MPa, with a reduction of 36.3%. Therefore, when there is a certain excess of Si, it can improve UTS and YS. The above results are consistent with the results by Zhang et al [19]. However, when the Mg/Si is 1.53, the alloy exhibits the lowest ductility because of the short skeletal shape and concentrated distribution of Mg₂Si phase. A detailed discussion is provided in the subsequent section about fracture analysis.

Solid solution strengthening, grain boundary strengthening [20], and thermal expansion mismatch strengthening [21] are the main strengthening mechanisms of the Al-Mg-Si alloys. Hence, it is necessary to quantitatively assess the contributions of various strengthening mechanisms in distinct alloys.

When the cooling rate of the solidification process reaches the sub-rapid solidification range of 10⁰ K·s⁻¹–10³ K·s⁻¹, Mg and Si can form a supersaturated solid solution in the Al-Mg-Si alloy. The solid solubility of Mg and Si elements in α-Al grains of the four alloys was examined by EDS and the results are shown in Table 2. According to Refs. [22, 23], the calculation of solid solution strengthening is expressed by Eq. (5):

$$\Delta\sigma_{ss} = \sum_i k_i c_i^{2/3} \quad (i=\text{Mg and Si}) \quad (5)$$

where k_i is the proportional factor of solution element i , $k_{\text{Mg}}=29.0$, $k_{\text{Si}}=66.3$, and c_i is the concentration of solid solution element i (wt.%). Then, substituting the results in Table 2 into Eq. (5), the solid solution strengthening ($\Delta\sigma_{ss}$) of Mg and Si elements was calculated, as shown in Table 3.

The contribution of grain boundary strengthening (σ_{gb}) can be supplemented by the Hall-Petch equation [24-26]:

$$\Delta\sigma_{gb} = \eta d^{-1/2} \quad (6)$$

where $\Delta\sigma_{gb}$ is the yield strength increment contributed by grain boundary strengthening, η is a factor related to many variables, based on the references [25, 27], $\eta=0.04 \text{ MPa}\cdot\text{m}^{1/2}$. d is the grain size. The average grain sizes of the α-Al matrix, as shown in Figs. 5(a1-d1), and the results of $\Delta\sigma_{gb}$ at different Mg/Si alloys are also listed in Table 3. On the whole, the contribution of grain boundary strengthening of the four Mg/Si alloys in this experiment is not prominent.

Table 2: Chemical compositions of α-Al phases in aluminum alloys with different Mg/Si mass ratios examined by EDS

Mg/Si	Mg (wt.%)	Si (wt.%)	Al (wt.%)
2.83	2.32	0.0	Bal.
1.91	1.57	0.34	Bal.
1.73	1.57	0.54	Bal.
1.53	1.37	1.03	Bal.

Table 3: Contribution of each strengthening mechanism and theoretical yield strength increment for alloys with different Mg/Si ratios

Mg/Si	$\Delta\sigma_{gb}$ (MPa)	$\Delta\sigma_{ss}$ (MPa)	$\Delta\sigma_{CTE}$ (MPa)	$\Delta\sigma_y$ (MPa)
2.83	6.14	50.8	18.67	75.61
1.91	6.27	71.5	21.05	98.82
1.73	5.52	82.8	24.74	113.06
1.53	6.03	103.0	17.22	126.25

For thermal expansion mismatch strengthening, Mg₂Si has a lower coefficient of thermal expansion (CTE, 7.5×10⁻⁶ K⁻¹), which is far from the base alloy thermal expansion coefficient (15.5×10⁻⁶ K⁻¹) [21]. Therefore, during the solidification process, due to the large CTE gap between Mg₂Si and the matrix, many dislocations will be generated, increasing the strength of the alloy. The thermal mismatch enhancement is expressed by Eq. (7):

$$\Delta\sigma_{CTE} = \beta G_m b \sqrt{\frac{12\Delta\alpha\Delta T V_p}{b d_p (1 - V_p)}} \quad (7)$$

where β is an intensity factor for Al, G_m is the shear modulus of the matrix alloy, b is the Burgers vector of α-Al, $\Delta\alpha$ is the CTE difference between Mg₂Si and the α-Al matrix, ΔT is the difference between the pouring temperature and room temperatures, and d_p and V_p are the average size and volume

fraction of the Mg₂Si phase, respectively. The values of the coefficients in Eq. (7) are shown in Table 4.

According to Eq. (7), the smaller the size and the larger the volume fraction of the Mg₂Si phase, the more obvious the strengthening effect on the alloy. The average size and volume fraction of the Mg₂Si phase are shown in Table 5.

Table 4: Values of variables in the thermal mismatch enhancement equation^[21]

β	G_m (GPa)	b (nm)	$\Delta\alpha$ (K ⁻¹)	ΔT (K)
1.25	25.8	0.286	8.0×10^{-6}	690

Table 5: Average size and volume fraction of Mg₂Si phase for alloys with different Mg/Si ratios

Mg/Si	Average size, d_p (nm)	Volume fraction, V_p (%)
2.83	13,508.4	19.29
1.91	12,089.6	21.37
1.73	9,683.9	23.13
1.53	13,934.7	17.33

The YS increment $\Delta\sigma_y$ ^[21, 28] can be expressed by Eq. (8), and the results of the four alloys are shown in Table 3.

$$\Delta\sigma_y = \Delta\sigma_{gb} + \Delta\sigma_{ss} + \Delta\sigma_{CTE} \quad (8)$$

From Table 3, it can be observed that grain boundary strengthening and thermal expansion mismatch strengthening contribute minimally to the strength of as-cast aluminum alloys.

In contrast, solid solution strengthening plays a more significant role. Notably, when the Mg/Si ratio is 1.53, the contribution of solid solution strengthening from Mg and Si elements to the increase in yield strength of the alloy peaks at 81.6%.

In addition, the morphology of Mg₂Si phase mainly depends on Mg/Si mass ratio, as shown in Fig. 7. When the ratios of Mg/Si are 2.83, 1.91, 1.73, and 1.53, the Mg₂Si morphologies are long skeletal shape, worm shape, short stick shape, and short skeletal shape, respectively. The corresponding elongation of the alloys is 5.31%, 4.82%, 2.83%, and 2.31%, respectively. Thus, the elongation of the alloy with the long skeletal Mg₂Si phase (Mg/Si=2.83) is the highest, and the alloy with the short skeletal Mg₂Si phase (Mg/Si=1.53) is the lowest.

Mg₂Si phases, as the main strengthening phases in Al-Mg-Si alloys, are harder and more brittle compared with α -Al matrix. During tensile deformation, strain/stress concentrates at the interface between Mg₂Si phases and the α -Al matrix, where crack initiation occurs. The morphology and distribution of Mg₂Si phases significantly influence the stress distribution at the interface of Mg₂Si phases and the α -Al matrix in Al-Mg-Si alloys. Uniformly distributed, short Mg₂Si phases result in minimal localized stress concentrations. The long skeletal Mg₂Si phases that are uniformly distributed can crack within some eutectic structures [Fig. 11(a)], this leads to a relatively higher elongation of 5.31%. In contrast, island-distributed Mg₂Si phases [as shown in Figs. 11(c) and (d)], even in short and stick-shaped or skeletal morphologies, cause cracks to form at the interface between the Mg₂Si phases and the α -Al matrix. These cracks propagate across the eutectic structures, leading to a reduction in elongation.

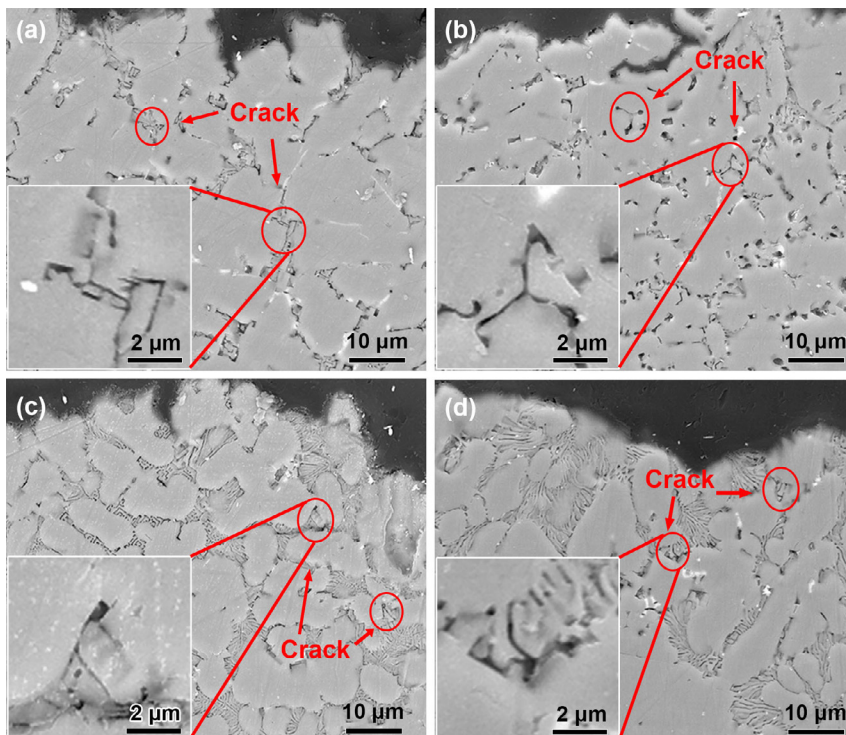


Fig. 11: Morphology and area fraction of cracked Mg₂Si phase near the fracture zone of different Mg/Si alloys: (a) 2.83; (b) 1.91; (c) 1.73; (d) 1.53

Figure 12 shows the microscopic morphology of tensile fractures at room temperature of alloys with different Mg/Si mass ratios. The fracture morphology of all the alloys shows dimples and cleavage planes of different sizes, so it is judged that the fracture type of all the alloys is ductile-brittle mixed-type fracture^[11]. The dimples in the alloys with Mg/Si mass ratios of 2.83 and 1.91 are large and densely distributed [Figs. 12(a, b)], which is consistent with a relatively higher elongation of the two alloys. Upon further reducing the Mg/Si to 1.73 and 1.53, the dimple size and the depth become smaller, the distribution is sparse [Fig. 12(c)], and the elongation of the alloy decreases.

Generally, the increase in the number of second-phase particles in the alloy can lead to a decrease in the plasticity of the alloy, and the dimples in the fracture also become smaller and shallower^[29]. Therefore, it is inferred that the enrichment of the Mg₂Si phases and Al(Fe, Mn)Si phases in the alloys with Mg/Si mass ratios of 1.73 and 1.53 is the main reason for the smaller and shallower fracture dimples. The EDS results show that the second phases at the bottom dimples [Figs. 12(e, f)] consist of the Mg₂Si phases and Al(Fe, Mn)Si phases, where stress concentration and crack initiation occur.

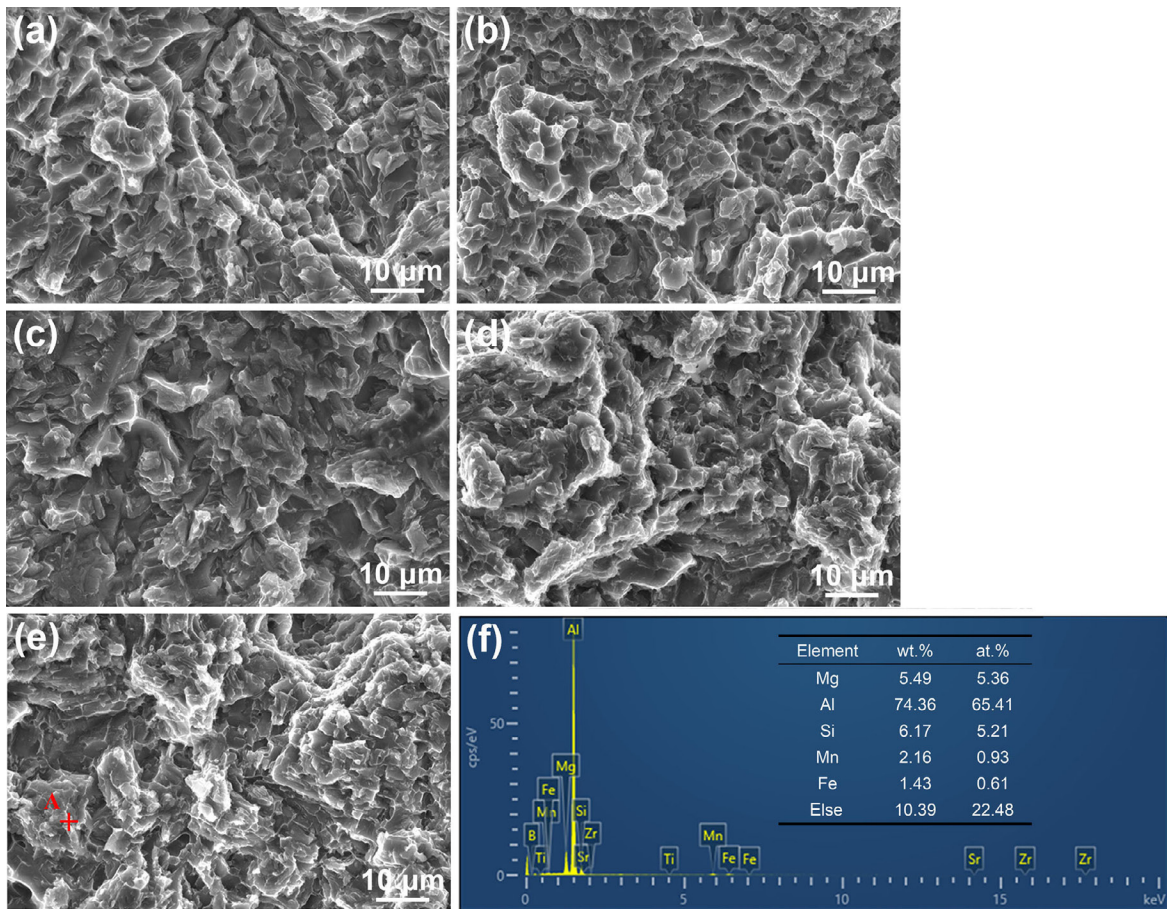


Fig. 12: SEM fracture morphologies of alloys with different Mg/Si ratios: (a) Mg/Si=2.83; (b) Mg/Si=1.91; (c) Mg/Si=1.73; (d) Mg/Si=1.53; (e) energy spectrum analysis of the alloy with an Mg/Si ratio of 1.53; (f) EDS results at Point A in (e)

4 Conclusions

The Al-Mg-Si alloys were prepared by vacuum copper mold suction casting under the sub-rapid solidification with a cooling rate of 291.3 K·s⁻¹. The effect of Mg/Si mass ratios (2.83, 1.91, 1.73, and 1.53) on the microstructure and mechanical properties of Al-Mg-Si as-cast alloys was investigated. The main conclusions are drawn as follows:

(1) The as-cast aluminum alloys with different mass ratios of Mg/Si exhibit fine equiaxed grains from 40.65 μm to 52.54 μm and SDAS from 7.83 μm to 8.10 μm. The size of grains and SDAS is not closely related to the Mg/Si ratio.

(2) As the mass ratio of Mg/Si decreases from 2.83 to 1.53,

there is a notable change in the morphology and distribution of Mg₂Si phases within the aluminum alloy. Specifically, the Mg₂Si phases transition from a long, skeletal shape to a shorter, skeletal form, and their distribution changes from a uniform pattern to an island-like, concentrated arrangement. This shift corresponds to a decrease in the alloy's elongation from 5.31% to 2.31%, indicating that the uniformly distributed Mg₂Si phases, even in long and skeletal morphologies, are more conducive to achieving a relatively higher elongation.

(3) The strengthening mechanisms of the as-cast Al-Mg-Si alloys are solid solution strengthening, grain boundary strengthening, and thermal expansion mismatch strengthening, and the contribution of solid solution strengthening plays a

major role. The alloy with Mg/Si of 1.53 among the four alloys has the highest mechanical properties with UTS of 320.6 MPa and YS of 249.9 MPa because of the highest solid solution strengthening of Mg and Si elements.

Acknowledgment

This work was supported by the WQ&UCS (Binzhou) Industrialization Research Institute.

Conflict of interest

The authors declare that they have no known competing financial interests or personal relationships that could have appeared to influence the work reported in this paper.

References

- [1] Papa I, Panico M, Carandente M, et al. Innovative joining technologies for lightweight material vehicles. Proceedings of the Institution of Mechanical Engineers, Sage Publications Ltd., 2024.
- [2] Zhao X, Wang P, Li T, et al. Gating system optimization of high pressure die casting thin-wall AlSi10MnMg longitudinal load-bearing beam based on numerical simulation. China Foundry, 2018,15(6): 436–442.
- [3] Chen J H, Liu C H. Microstructure evolution of precipitates in AlMgSi (Cu) alloys. The Chinese Journal of Nonferrous Metals, 2011, 21(10): 2352–2360.
- [4] Trudonoshyn O, Rehm S, Randelzhofer P, et al. Improvement of the high-pressure die casting alloy Al-5.7Mg-2.6Si-0.7Mn with Zn addition. Materials Characterization, 2019, 158: 109959.
- [5] Ji S X, Watson D, Wang Y, et al. Effect of Ti addition on mechanical properties of high pressure die cast Al-Mg-Si alloys. In: Sixth International Light Metals Technology Conference (LMT2013), Old Windsor, United Kingdom, 2013, 765: 23–27.
- [6] Zhu C, Zhu Q F, Ban C Y, et al. Effect of solid solution state of zirconium and Al₃Zr (L12) precipitates on the recrystallization behavior of Al-0.2 wt.% Zr alloy. Materials Science and Engineering Technology, 2020, 51(12): 1630–1639.
- [7] Lim Y P, Yeo W H. The effects of scandium on A356 aluminium alloy in gravity die casting. Materials Research Innovations, 2014, 18(6): 395–399.
- [8] Gupta A K, Lloyd D J, Court S A. Precipitation hardening in Al-Mg-Si alloys with and without excess Si. Materials Science and Engineering: A, 2001, 316(1–2): 11–17.
- [9] Li J F, Zheng Z Q, Li S C, et al. Simulation study on function mechanism of some precipitates in localized corrosion of Al alloys. Corrosion Science: The Journal on Environmental Degradation of Materials and Its Control, 2007, 49(6): 2436–2449.
- [10] Fan B Y, Li Y D, Li X, et al. Effects of w(Mg)/w(Si) ratio on microstructure, thermal and mechanical properties of Al-Mg-Si alloys. Special Casting & Nonferrous Alloys, 2021, 41(2): 168–173. (In Chinese)
- [11] Ben N J, Sun Y, Zhou P F. Effect of Mg content on microstructure evolution and properties of AlSiMg alloy. Foundry, 2020, 69(9): 929–933. (In Chinese)
- [12] Chen G, Fu H Z. Non-equilibrium solidification of new metal materials. Beijing: Science Press, 2004: 1–2. (In Chinese)
- [13] Cheng T Y, Zhang S H. Rapid solidification technology and new alloys. Beijing: China Aerospace Publishing House, 1990: 26–27. (In Chinese)
- [14] Li Y Z. Rapid solidification technology and materials. Beijing: National Defense Industry Press, 1993: 3–4. (In Chinese)
- [15] Huang Z L, Wang K, Zhang Z M, et al. Effects of Mg content on primary Mg₂Si phase in hypereutectic Al-Si alloys. Transactions of Nonferrous Metals Society of China, 2015, 25(10): 3197–3203.
- [16] Yan X J, Sui Y D, Zhou H, et al. Influence of the Mg content on the microstructure and mechanical properties of Al-xMg-2.0Si-0.6Mn alloy. Journal of Materials Research and Technology, 2023, 23: 3880–3891.
- [17] Baldan R, Malavazi J, Couto A A. Microstructure and mechanical behavior of Al9Si0.8Fe alloy with different Mn contents. Materials Science and Technology, 2017, 33(10): 1192–1199.
- [18] Sang Y, Chen J H, Liu C H, et al. A comparison study of precipitation behaviors in three Al-Mg-Si alloys with different Mg/Si composition ratios. Journal of Chinese Electron Microscopy Society, 2012, 31(5): 384–390.
- [19] Zhang J X, Gao A H. Influence of surplus Si on microstructure and properties of 6063 aluminum alloy. Special Casting & Non-ferrous Alloys, 2008(2): 148–149, 81. (In Chinese)
- [20] Wang Y, Deng Y L, Dai Q S, et al. Microstructures and strengthening mechanisms of high Fe containing Al-Mg-Si-Mn-Fe alloys with Mg, Si and Mn modified. Materials Science and Engineering: A, 2021, 803: 140477.
- [21] Li J Y, An Q, Wu S S, et al. Relationship of Mg₂Si morphology with Mg₂Si content and its effect on properties of in-situ Mg₂Si/Al-Cu composites. Journal of Alloys and Compounds, 2019, 808: 151771.
- [22] Myhr O R, Grong O, Andersen S J. Modelling of the age hardening behaviour of Al-Mg-Si alloys. Acta Materialia, 2001, 49(1): 65–75.
- [23] Yang M J, Chen H N, Orekhov A, et al. Quantified contribution of β^{*} and β' precipitates to the strengthening of an aged Al-Mg-Si alloy. Materials Science and Engineering: A, 2020, 774: 138776.
- [24] Petch N J. The cleavage strength of polycrystals. Journal of Iron and Steel Institution, 1953, 174: 25–28.
- [25] Mcelroy R J, Szkopiak Z C. Dislocation-substructure-strengthening and mechanical – Thermal treatment of metals. International Metallurgical Reviews, 1972, 17(1): 175–202.
- [26] Yang C K, Zhou Y C. Mechanical properties of Ti₂SnC particulate reinforced Cu matrix composites. Acta Metallurgica Sinica, 2003, 1: 99–103.
- [27] Wyrzykowski J W, Grabski M W. The Hall-Petch relation in aluminum and its dependence on the grain-boundary structure. Philosophical Magazine: A, 1986, 53(4): 505–520.
- [28] Feng L, Li J G, Mao Y Z. Strengthening and toughening mechanism of high-Mg low-Sc Al-Mg-Sc-Zr alloy. Rare Metal Materials and Engineering, 2019, 48(9): 2857–2863.
- [29] Tillová E, Chalupová M, Závodská D, et al. Effect of Al₅FeSi phases in secondary AlZn10Si8Mg cast alloys on mechanical properties and fracture surface. Manufacturing Technology, 2018, 18(6): 1034–1040.